Journal of Physics:
Condensed Matter

PAPER

Ultrafast structural transition and electron-phonon/phonon–phonon coupling in antimony revealed by nonadiabatic molecular dynamics

To cite this article: Meng Niu *et al* 2025 *J. Phys.: Condens. Matter* **37** 045401

IOP Publishing Journal of Physics: Condensed Matter
J. Phys.: Condens. Matter **37** (2025) 045401 (7pp) https://doi.org/10.1088/1361-648X/ad8696

Ultrafast structural transition and electron-phonon/phonon–phonon coupling in antimony revealed by nonadiabatic molecular dynamics

Meng Niu, Shun-Yao Qin, Bai-Qian Wang, Nian-Ke Chen* and Xian-Bin Li*

State Key Laboratory of Integrated Optoelectronics, College of Electronic Science and Engineering, Jilin University, 130012 Changchun, People's Republic of China

E-mail: chennianke@jlu.edu.cn and lixianbin@jlu.edu.cn

Received 15 August 2024, revised 2 October 2024
Accepted for publication 14 October 2024
Published 1 November 2024

Abstract

Real-time time-dependent density-functional theory molecular dynamics (rt-TDDFT-MD) reveals the nonadiabatic dynamics of the ultrafast photoinduced structural transition in a typical phase-change material antimony (Sb) with Peierls distortion (PD). As the excitation intensity increases from 3.54% to 5.00%, three distinct structural transition behaviors within 1 ps are observed: no PD flipping, nonvolatile-like PD flipping, and nonstop back-and-forward PD flipping. Analyses on electron-phonon and phonon–phonon couplings indicate that the excitation-activated coherent A_{1g} phonon mode by electron-phonon coupling drives the structural transition within several hundred femtoseconds. Then, the energy of coherent motions are transformed into that of random thermal motions via phonon–phonon coupling, which prevents the A_{1g}-mode-like coherent structure oscillations. The electron-phonon coupling and coherent motions will be enhanced with increasing the excitation intensity. Therefore, a moderate excitation intensity that can balance the coherent and decoherent thermal movements will result in a nonvolatile-like PD flipping. These findings illustrate important roles of nonadiabatic electron-phonon/phonon–phonon couplings in the ultrafast laser-induced structural transitions in materials with PD, offering insights for manipulating their structures and properties by light.

Keywords: photoinduced structural transition, electron-phonon/phonon–phonon coupling, antimony, time-dependent density-functional theory molecular dynamics, Peierls distortion

Ultrafast laser-induced structural transition is not only a key topic of light-matter interactions [1–3] but also plays an important role in optoelectronic applications, such as device fabrication [4, 5] and optical storage [6, 7]. Understanding the mechanism of the ultrafast transition is of great significance for both scientific research and device-performance improvements. Antimony (Sb) is a phase-change material (PCM) for both optical [8] and electronic memory devices [9, 10]. As a monoelement material, it can avoid phase separation and thus improve the endurance of the device. By incorporating a substrate, Sb can undergo a transformation from a non-metal to a metal [11, 12]. Moreover, Sb is a semimetal with a rhombohedral phase structure, exhibiting lattice distortion along the [001] direction of crystal unit cell due to Peierls instability. Many theoretical and experimental studies have demonstrated that materials with Peierls distortion (PD) are typical platforms for the studies of light-induced non-thermal structural transitions

* Authors to whom any correspondence should be addressed.

[13–15]. For Sb, it has already been experimentally confirmed that A_{1g} phonon modes can be activated by ultrafast lasers [16, 17]. According to the mechanism of displacive excitation of coherent phonons (DECP) [18], activation of A_{1g} phonon is quite possible to induce a phase or structural transition.

Usually, time-resolved electron diffraction [19], and x-ray diffraction [20] are powerful techniques for the study of the ultrafast structural transition. Unfortunately, such expensive techniques still cannot directly see atomic dynamics due to the lack of real-time real-space atomic pictures. In contrast, first-principles calculations and molecular dynamics have shown great potential in revealing electronic and atomic mechanisms. For example, adiabatic molecular dynamic simulations based on an analysis of laser-excited potential energy surfaces (PESs) indicate that femtosecond laser can induce non-thermal structural transitions in Sb from a PD structure to another PD structure but with opposite long/short bond distribution [21]. However, the nonadiabatic electron-phonon and phonon–phonon couplings, which are absent in previous adiabatic simulations, should play significant roles in the ultrafast laser-induced nonequilibrium states [22–24]. Therefore, it is worth clarifying the influence of the nonadiabatic interactions on the dynamics of its ultrafast laser-induced structural transitions. Recently, real-time time-dependent density-functional theory molecular dynamics (rt-TDDFT-MD) [25] has been proven to be an effective approach to evaluating the nonadiabatic electron-phonon/phonon–phonon interactions in laser-induced structural transitions [26–28].

In this work, we study photoinduced structural transitions of Sb using the rt-TDDFT-MD, which reveals the influence of electron-phonon/phonon–phonon interaction during the process. By gradually varying the excitation intensity, a critical intensity range for nonvolatile-like PD flipping is identified. If the intensity is higher, the structure will flip back and forth in form of coherent oscillations. The analyses on nominal and thermal temperatures indicate that the electron-phonon coupling triggered coherent A_{1g} phonon mode drives the structural transitions, while the random thermal motions prevent the transition by disrupting the coherent motions through phonon–phonon couplings. The duration of the coherent motions can last several hundred femtoseconds or longer, depending on the excitation intensity. The higher the excitation intensity, the stronger the coherent motions. Therefore, a moderate excitation intensity can lead to a balance between coherent and decoherent motions and thus result in non-volatile PD flipping in Sb. The results reveal the important roles of electron-phonon/phonon–phonon couplings in the ultrafast laser-induced structural transition of PD materials, which may guide the manipulation of their structures and properties by light.

Figure 1(a) shows the crystalline structure of rhombohedral Sb. Each atom has five valence electrons, three of which form bonds with adjacent atoms and two of which form a lone pair [23]. The distance between nearest neighbor atoms (for short bond) is 2.96 Å, while the distance between the next nearest neighbor atoms (for long bond) is 3.41 Å. As a result, the inter-layer distances along the z direction are separated into

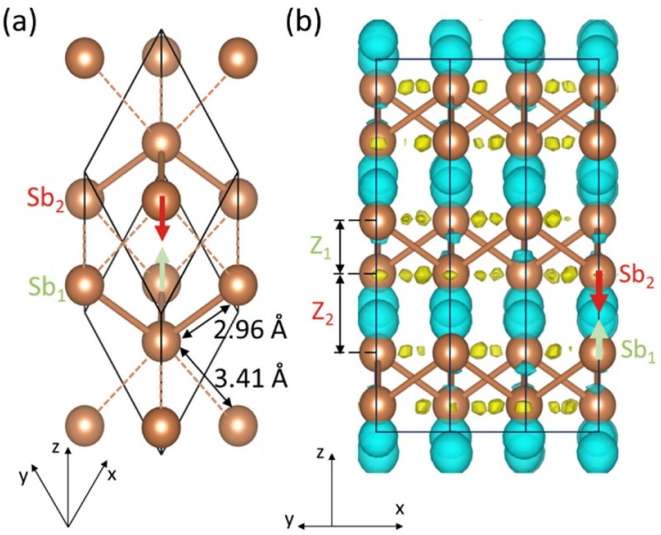

Figure 1. (a) Primitive cell of rhombohedral Sb. The length of the solid line (for short bond) is 2.96 Å while the length of the dotted line (for long bond) is 3.41 Å. (b) A crystal supercell of Sb and the charge density difference between after and before electron excitation ($\rho_{\text{excitation}}-\rho_{\text{ground}}$) of 5.00% valence electrons. The isosurface is 0.0012 e/a_0^3, where a_0 is the Bohr radius. yellow and blue areas indicate the increase and decrease of charge density, respectively. The green and red arrows represent respectively the upward and downward force for Sb_1 and Sb_2 atoms under excitation.

two types including the short and long distances, as indicated by Z_1 and Z_2 in figure 1(b). The difference between these distances is also characterized by the so-called Peierls parameter [21].

When the electrons are excited from the valence band to the conduction band, the electrons are mainly removed from lone-pair electrons to antibonding states (see figure 1(b)). Note that a small number of electrons are also removed from bonding states, though this change is too subtle to be detected in figure 1(b). The excitation-induced charge transfer instantly breaks the ground-state equilibrium between electrons and atoms, producing resultant forces on atoms. The net forces within the x-y plane in figure 1(b) are canceled out due to the symmetric structure. In contrast, the symmetry breaking along the z-direction results in net forces along the z-axis. Specifically, the forces on atoms labeled Sb_1 are directed upward, while the forces on atoms labeled Sb_2 are directed downward (see the green and red arrows in figure 1(b)). In fact, if the atoms move along the z-direction according to the excitation driving force, the motion should be strongly related to the A_{1g} phonon mode, where Sb_1 and Sb_2 move out of phase along the z-directions.

Next, we carry out rt-TDDFT-MD to study atomic dynamics of Sb under optical excitation. Indeed, the MD simulations reflect the activation of A_{1g} mode under excitation. If the excitation intensity is low, it can only activate the A_{1g} mode rather than a structural transition [29]. Such a phonon activation is the well-known DECP [18, 30, 31]. Here, we only focus on the relatively large excitation intensities (see

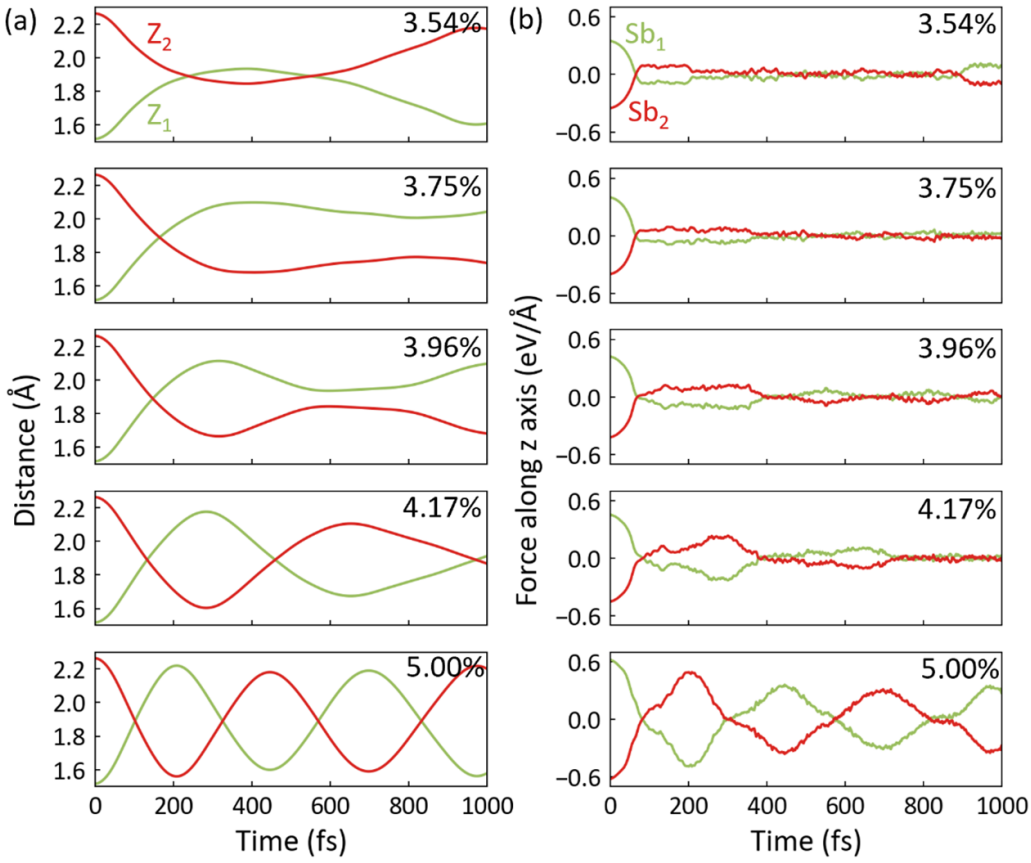

Figure 2. (a) Time evolution of structural parameters (Z_1 and Z_2) under different excitation intensities in Sb. (b) Time evolution of average forces along the z-axis for two types of Sb atoms (Sb_1 and Sb_2). The parameters and atomic types have been defined in figure 1(b) .

the definition in **Method** section) that can induce structural transitions. By gradually adjusting the excitation intensities, we identified a critical intensity (3.54% of the valence electrons) that triggers a structural transition involving atomic layer flipping. Figure 2(a) shows the time evolutions of the Z_1 and Z_2, which can characterize the PD, under various excitation intensities between 3.54% and 5.00%. For the intensity of 3.54%, the direction of PD is reversed after 210 fs. When the excitation intensity slightly increases to 3.75% and 3.96%, nonvolatile-like PD flipping can be observed after 160 fs and 150 fs, respectively. If the intensity increases to 5.00%, the back-and-forward flipping occurs without stopping during the whole 1000 fs simulation. These coherent structural transitions can be explained by the gradual change of the double-well PES to the single-well PES as the excitation intensity increases [21].

Figure 2(b) tracks the average atomic forces along the direction of PD (i.e. z-axis), which can help to understand the dynamics of the coherent atomic motions along the z-axis. For all the cases of different excitation intensities, initial forces on atoms labeled Sb_1 and Sb_2 are upward and downward respectively (corresponding to positive and negative values in figure 2(b)). The initial force increases with excitation intensity. When the intensity is below 4.17%, the average force is significantly reduced at the end of the simulation. In contrast, when the intensity is larger than 5.00%, the average force can exist even at the end of the simulation (i.e. 1000 fs), explaining its nonstop back-and-forward PD flipping by this strong coherent driving force in this period. It is worth noting that the ultrafast structural transition in Sb under 5.00% excitation differs from that in GeTe under the same excitation intensity [14], despite both GeTe and Sb having A7 rhombohedral structures with PD. In the case of GeTe, the A7 structure transformed into a cubic structure without PD within 1 ps owing to the decay of coherent oscillations [14]. The difference suggests that the decoherence effect in single-element Sb is much weaker than that in GeTe. Perhaps this is because GeTe contains two different types of atoms, whereas Sb is composed of only one kind of element.

Next, we try to understand the role of electron-phonon and phonon–phonon coupling effects in the laser-induced ultrafast structural transition in Sb. Generally, when a material is excited by a femtosecond laser pulse, the energy of light will first be injected into its electronic system and then gradually be transferred to its lattice system via electron-phonon coupling [32, 33]. Therefore, the time evolution of lattice temperature can reflect the electron-phonon coupling effect. The black lines in figure 3 represent a nominal temperature, which is the average temperature of all kinds of atomic motions, including excitation-induced coherent motions and random thermal motions. For all the intensities, the nominal temperature increases

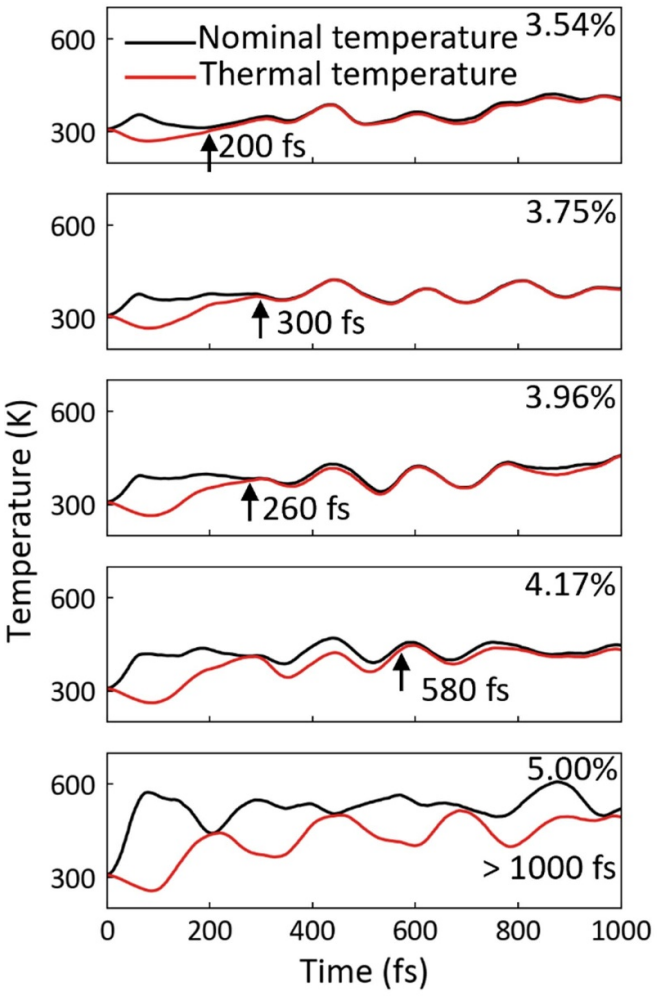

Figure 3. Time evolution of lattice temperatures under different excitation intensities. The black and red lines represent the nominal and thermal temperatures, respectively.

significantly at the beginning of 100 fs due to the activation of A_{1g} phonons via DECP electron-phonon coupling [18], see the discussion later. It is clear that as the excitation intensity increases, the electron-phonon coupling becomes stronger.

Note that the nominal temperature also contains the contribution from coherent atomic movements. To further evaluate the dynamics of coherent movements and lattice thermalization separately, we define a thermal temperature contributed by pure random thermal motions. Then, the thermal temperature can be calculated by excluding the coherent atomic movements from the nominal temperature (see **Method** section for more details). The results are indicated by the red lines in figure 3. The separation of the nominal and thermal temperatures confirms again that the initial temperature elevation results from coherent motions rather than random thermal motions. Then, the thermal temperature gradually increases with time and later is close to the nominal temperature. The coincidence of the two temperatures indicates the lattice has reached its thermal quasi-equilibrium state and the coherent motion has basically stopped. In other words, the energy is transferred from the coherent A_{1g} phonon mode to other phonon modes via phonon–phonon coupling. Thus, the comparison between thermal temperature and nominal temperature can be used to measure the time scale of phonon–phonon coupling. The time required for the two temperatures to converge, as indicated by the black arrow in figure 3, indicate the duration of coherent motions. The duration approximately increases with excitation intensities. For the excitation intensities of 3.54%–4.17%, it is as fast as several hundred femtoseconds. However, if the excitation reaches 5.00%, the coherent motion persists throughout the entire simulation period (1000 fs). After the beginning 100 fs, the nominal temperature only increases slightly suggesting the energy transfer from the electronic system to the lattice system (characterized by electron-phonon coupling) during that stage is small. Therefore, it can be deduced that the lattice thermalization and the decoherence effect here are mainly realized by phonon–phonon coupling.

To confirm the key phonon modes during the structural transitions, the trajectories of the rt-TDDFT-MD simulations are projected to the phonon modes of Sb at the Γ point. The projected intensity is defined as $\sum_j e_i \cdot \mu_j$, where μ_j is the displacement vector of atom j from its original position at $t = 0$ fs and e_i is the ith phonon eigenvector at the Γ point [22]. A conventional cell of Sb with six atoms is used to calculate the phonon eigenvectors. Figure 4(a) schematically shows the atomic displacements of two main phonon modes (i.e. A_{1g} and E_g modes). Figure 4(c) shows the time evolution of the projected intensity of the phonon modes during the MD simulations. Indeed, the A_{1g} mode is the most predominant phonon mode activated by laser excitation, which is consistent with the previous analyses on the Peierls parameter and atomic forces. At the relatively low excitation intensity of 3.54%, the in-plane-direction E_g mode (red line in figure 4(c)) is also activated in addition to the z-direction A_{1g} mode. However, as the excitation intensity increases, the A_{1g} mode gains prominence but the E_g mode gradually becomes weaker. Figure 4(b) provides a quantitative representation of this trend. Here, the amplitude of each phonon mode is defined as the absolute value of the maximum of the projected intensity in figure 4(c). By combining the structural transitions shown in figure 2(a) with the coherence effect revealed in figure 3, we deduce that the A_{1g} mode is the driving force behind the coherent structural transitions, while other phonon modes may hinder the transition by disrupting coherent motions. Therefore, suitable excitation intensities like 3.75% and 3.96% can induce balanced states between the A_{1g} mode and the other modes, thus leading to the nonvolatile-like PD flipping as shown in figure 2(a). When the excitation intensity is further larger, the balance states are disrupted, resulting in strong, nonstop back-and-forth PD flipping driven by the A_{1g} mode.

In conclusion, we have studied the structural dynamics of Sb under ultrafast laser excitation by the non-adiabatic rt-TDDFT-MD method. As the excitation intensity increases from 3.54% to 5.00%, the structural transitions in Sb within

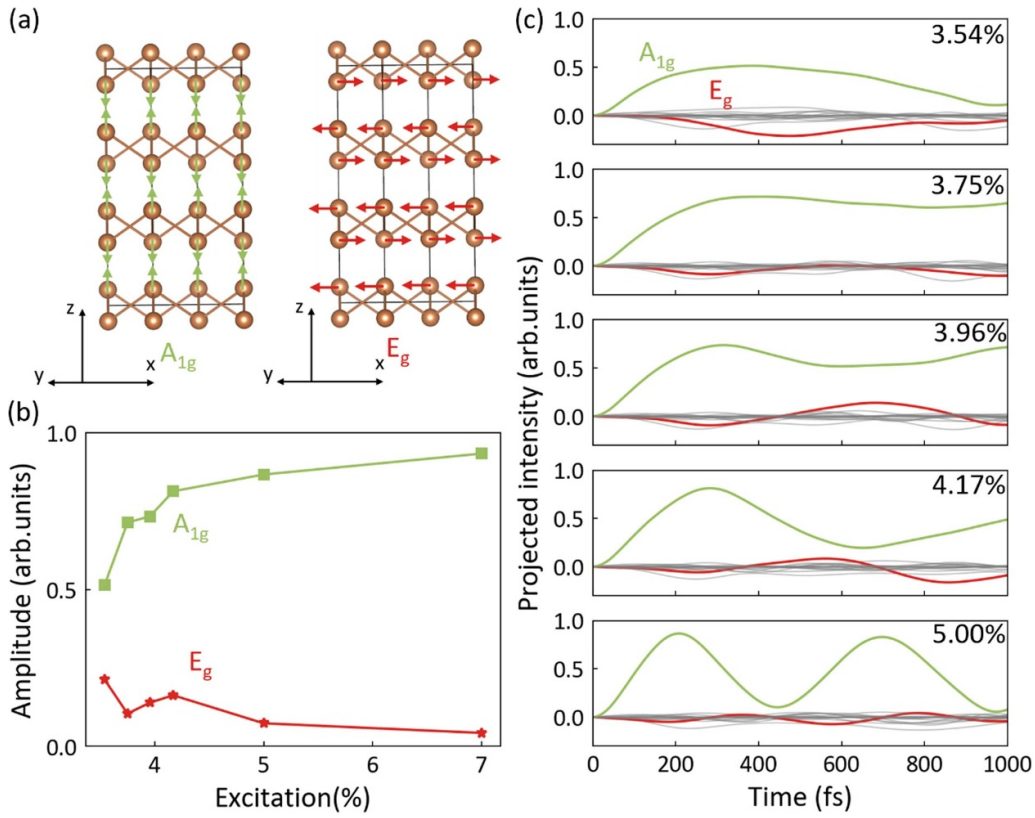

Figure 4. (a) Vibrational eigenvectors of two dominant phonon modes. The green and red arrows indicate the atomic displacement direction of the A_{1g} and E_g phonon modes, respectively. (b) The phonon amplitude of the A_{1g} and the E_g modes under different excitations, extracted from molecular dynamics. (c) Projected atom displacements (with time) onto vibrational eigenmodes of phonons. The red line, green line, and gray lines represent the E_g mode, the A_{1g} mode, and other modes, respectively.

1 ps exhibit three scenarios: no PD flipping, nonvolatile-like PD flipping, and continuous back-and-forth PD flipping. The structural transition is driven by coherent atomic movements along the *z*-direction, aligning with the A_{1g} phonons. By separating coherent motions and random thermal motions, a thermal temperature (different from the nominal temperature) is defined to evaluate the electron-phonon/phonon–phonon couplings. The analyses indicate that the energy transfers rapidly from the electronic system to the lattice system within ∼100 fs after excitation. During this stage, the coherent motions are dominant. After this stage, the energy of the coherent A_{1g} phonons gradually transfers into the ones of other phonon modes via phonon–phonon coupling. As the excitation intensity increases, both the duration and amplitude of the coherent motions increase. Therefore, a moderate excitation intensity can realize a non-volatile PD flipping owing to a balance between coherent motions and random thermal motions. In contrast, a high excitation intensity will lead to very strong A_{1g} phonon oscillations thus resulting in a nonstop PD flipping within 1000 fs. We expect that the special phonon behaviors and coherent dynamics induced by optical excitation are critical to manipulating ultrafast structural transition of materials with PD. The current study will also facilitate the exploration of advanced optoelectronic devices that rely on light-induced ultrafast structural and signal transitions.

1. Method

1.1. Computational details

In the present work, the calculations are performed using the time-dependent *ab initio* package as implemented in SIESTA [34] with norm-conserving Troullier–Martins pseudopotentials [35] and PBE functional [36]. The plane wave energy cutoff is 200 Ry and the local basis set with double-ζ polarized orbitals is employed. In geometry optimization, the energy convergence criterion was set to be 10^{-5} eV, and the ion positions were optimized until the atomic forces were below 10^{-2} eV Å^{-1}. Lattice dynamics calculations were performed with the Phonopy package [37]. The force constant matrices were calculated using a $4 \times 4 \times 2$ supercell with 192 atoms. The rt-TDDFT-MD calculations are performed with the NVE ensemble. The coupling between atomic and electronic motions is governed by the Ehrenfest approximation [38]. Although the Ehrenfest approximation does not include the spontaneous phonon emission [39], the rt-TDDFT MD based on this approximation is suitable to describe the structural transitions. And, it has been widely used in the study of photoinduced structural transition and has successfully explained various experimental observations [28, 40]. The time step is 0.024 fs, and the equilibrium state of a ground-state MD at 300 K is used as the input. In rt-TDDFT-MD, we

use a 192-atom supercell and the Γ point for Brillouin zone integration.

We simulate the excitation of the electrons by changing the occupation of the corresponding KS states involved in the photo-excitation [41]. Excitation in this work is achieved by moving electrons from the valence band to the conduction band to achieve the effect of photoexcitation. The quantity of excitation intensity is defined as the ratio of excited electrons to the number of valence electrons.

1.2. Nominal and thermal temperatures

The nominal temperature is defined as $T = (T_1 + T_2)/2 = (\frac{m{v_1}^2}{3k_B} + \frac{m{v_2}^2}{3k_B})/2$, 1 and 2 represent the two types of atoms labeled Sb_1 and Sb_2 in figure 1(b).

Here, ${\boldsymbol{v}_1}^2$ can be expanded to

$$\begin{aligned}{\boldsymbol{v}_1}^2 &= \frac{\sum_{i=1}^{n}{\boldsymbol{v}_{1i}}^2}{n} = \frac{\sum_{i=1}^{n}\left(\overline{\boldsymbol{v}_1} + \boldsymbol{\Delta v}_{1i}\right)^2}{n} \\ &= \overline{\boldsymbol{v}_1}^2 + \frac{2\overline{\boldsymbol{v}_1}\cdot\sum_{i=1}^{n}\boldsymbol{\Delta v}_{1i}}{n} + \frac{\sum_{i=1}^{n}{\boldsymbol{\Delta v}_{1i}}^2}{n}.\end{aligned}$$

$\boldsymbol{v}_{1i}$ represents the velocity of ith Sb_1 atom, $\overline{\boldsymbol{v}_1}$ represents the average velocity of Sb_1, $\boldsymbol{\Delta v}_{1i} = \boldsymbol{v}_{1i} - \overline{\boldsymbol{v}_1}$, n represents the number of Sb_1. The second term in the right hand of the formula, $\sum_{i=1}^{n}\boldsymbol{\Delta v}_{1i} = \sum_{i=1}^{n}\left(\boldsymbol{v}_{1i} - \overline{\boldsymbol{v}_1}\right) = 0$, so that, ${\boldsymbol{v}_1}^2 = \overline{\boldsymbol{v}_1}^2 + \frac{\sum_{i=1}^{n}{\boldsymbol{\Delta v}_{1i}}^2}{n}$. The first term of the equation can be considered to be caused by coherent motion, and the second term can be considered to be the influence of disordered thermal motions. Similarly, ${\boldsymbol{v}_2}^2 = \overline{\boldsymbol{v}_2}^2 + \frac{\sum_{i=1}^{n}{\boldsymbol{\Delta v}_2}^2}{n}$. Therefore, the thermal temperature can be defined as

$$T_{\text{thermal}} = \frac{m}{6k_B}\left(\frac{\sum_{i=1}^{n}{\Delta v_{1i}}^2}{n} + \frac{\sum_{i=1}^{n}{\Delta v_{2i}}^2}{n}\right).$$

Data availability statement

All data that support the findings of this study are included within the article (and any supplementary files).

Acknowledgments

This work was supported by the National Science and Technology Major Project (Grant No. 2022ZD0117600), National Natural Science Foundation of China (Grant Nos. 12274180 and 12274172), the Natural Science Foundation of Jilin Province (20230101007JC), and the Fundamental Research Funds for the Central Universities. High-Performance Computing Center (HPCC) at Jilin University is also acknowledged.

ORCID iDs

Meng Niu https://orcid.org/0009-0004-8398-3213
Xian-Bin Li https://orcid.org/0000-0002-0046-2016

References

[1] Guan M, Chen D, Chen Q, Yao Y and Meng S 2023 *Phys. Rev. Lett.* **131** 256503
[2] Zheng Q, Saidi W A, Xie Y, Lan Z, Prezhdo O V, Petek H and Zhao J 2017 *Nano Lett.* **17** 6435–42
[3] Liu W H, Gu Y X, Wang Z, Li S S, Wang L W and Luo J W 2023 *Phys. Rev. Lett.* **130** 146901
[4] Zhao J H, Li X B, Chen Q D, Chen Z G and Sun H B 2020 *Mater. Today Nano* **11** 100078
[5] Han F, Gu S, Klimas A, Zhao N, Zhao Y and Chen S C 2022 *Science* **378** 1325–31
[6] Ríos C, Stegmaier M, Hosseini P, Wang D, Scherer T, Wright C D, Bhaskaran H and Pernice W H P 2015 *Nat. Photon.* **9** 725–32
[7] Li T *et al* 2022 *Adv. Mater.* **34** 2108261
[8] Cheng Z, Milne T, Salter P, Kim J S, Humphrey S, Booth M and Bhaskaran H 2021 *Sci. Adv.* **7** eabd7097
[9] Shen X, Zhou Y, Zhang H, Deringer V L, Mazzarello R and Zhang W 2023 *Nanoscale* **15** 15259–67
[10] Chen Y *et al* 2022 *Mater. Today Phys.* **22** 100584
[11] Gorodetsky D A, Mel'nik Y P, Proskurin D P and Usenko V A 2004 *Phys. Solid State* **46** 1940–8
[12] Proskurin D, Nikolaychik A, Koval I F and Yakovkin I N 2006 *Phys. Status Solidi* b **243** 584–91
[13] Ning H, Mehio O, Lian C, Li X, Zoghlin E, Zhou P, Cheng B, Wilson S D, Wong B M and Hsieh D 2022 *Phys. Rev.* B **106** 205118
[14] Chen N K, Li X B, Bang J, Wang X P, Han D, West D, Zhang S and Sun H B 2018 *Phys. Rev. Lett.* **120** 185701
[15] Chen N K, Bang J, Li X B, Wang X P, Wang D, Chen Q D, Sun H B and Zhang S 2020 *Phys. Rev.* B **102** 184115
[16] Garrett G A, Albrecht T F, Whitaker J F and Merlin R 1996 *Phys. Rev. Lett.* **77** 3661–4
[17] Ishioka K, Kitajima M and Misochko O V 2008 *J. Appl. Phys.* **103** 123505
[18] Zeiger H J, Vidal J, Cheng T K, Ippen E P, Dresselhaus G and Dresselhaus M S 1992 *Phys. Rev.* B **45** 768–78
[19] Mironov B N, Kompanets V O, Aseev S A, Ischenko A A, Kochikov I V, Misochko O V, Chekalin S V and Ryabov E A 2017 *J. Exp. Theor. Phys.* **124** 422–8
[20] Matsubara E *et al* 2016 *Phys. Rev. Lett.* **117** 135501
[21] Bauerhenne B, Zijlstra E S and Garcia M E 2017 *Appl. Phys.* A **123** 608
[22] Guan M X, Liu X B, Chen D Q, Li X Y, Qi Y P, Yang Q, You P W and Meng S 2022 *Phys. Rev. Lett.* **128** 015702
[23] Shinohara Y, Sato S A, Yabana K, Iwata J I, Otobe T and Bertsch G F 2012 *J. Chem. Phys.* **137** 22A527
[24] Lian C, Zhang S B and Meng S 2016 *Phys. Rev.* B **94** 184310
[25] Runge E and Gross E K U 1984 *Phys. Rev. Lett.* **52** 997–1000
[26] Liu X B, Hu S Q, Chen D, Guan M, Chen Q and Meng S 2022 *Nano Lett.* **22** 4800–6
[27] Chen N K, Han D, Li X B, Liu F, Bang J, Wang X P, Chen Q D, Wang H Y, Zhang S and Sun H B 2017 *Phys. Chem. Chem. Phys.* **19** 24735–41
[28] Lian C, Guan M, Hu S, Zhang J and Meng S 2018 *Adv.Theory Simul.* **1** 1800055
[29] Misochko O V 2016 *J. Exp. Theor. Phys.* **123** 292–302
[30] Mazin I I, Liechtenstein A I, Jepsen O, Andersen O K and Rodriguez C O 1994 *Phys. Rev.* B **49** 9210–3
[31] Melnikov A A, Misochko O V and Chekalin S V 2011 *Phys. Lett.* A **375** 2017–22
[32] Carpene E 2006 *Phys. Rev.* B **74** 024301
[33] Chen J K, Tzou D Y and Beraun J E 2006 *Int. J. Heat Mass Transfer* **49** 307–16
[34] Meng S and Kaxiras E 2008 *J. Chem. Phys.* **129** 054110

[35] Troullier N and Martins J L 1991 *Phys. Rev.* B **43** 1993–2006
[36] Perdew J P, Burke K and Ernzerhof M 1997 *Phys. Rev. Lett.* **78** 1396
[37] Togo A and Tanaka I 2015 *Scr. Mater.* **108** 1–5
[38] Alonso J L, Andrade X, Echenique P, Falceto F, Prada-Gracia D and Rubio A 2008 *Phys. Rev. Lett.* **101** 096403
[39] le Page J, Mason D R and Foulkes W M C 2008 *J. Phys.: Condens. Matter* **20** 125212
[40] Guan M, Chen D, Hu S, Zhao H, You P and Meng S 2022 *Ultrafast Sci.* **2022** 9767251
[41] Ma W, Zhang J, Yan L, Jiao Y, Gao Y and Meng S 2016 *Comput. Mater. Sci* **112** 478–86